Accurate modeling of split ring metamaterial lenses for magnetic resonance imaging applications

Cite as: J. Appl. Phys. **105**, 024907 (2009); https://doi.org/10.1063/1.3067788
Submitted: 12 August 2008 . Accepted: 04 December 2008 . Published Online: 27 January 2009

L. Jelinek, R. Marqués, and M. J. Freire

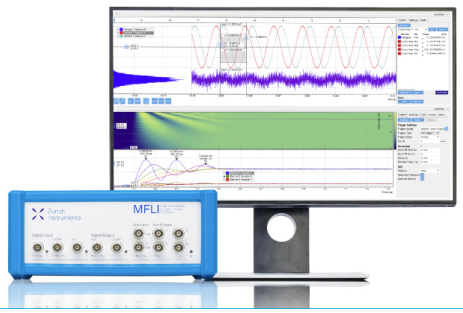

Accurate modeling of split ring metamaterial lenses for magnetic resonance imaging applications

L. Jelinek,[a] R. Marqués,[b] and M. J. Freire[c]
Departamento de Electrónica y Electromagnetismo, Universidad de Sevilla, Sevilla 41012, Spain

(Received 12 August 2008; accepted 4 December 2008; published online 27 January 2009)

The usefulness of thin split ring metamaterial slabs for imaging applications, including magnetic resonance imaging applications, has attracted some attention in the past years. However, the small number of unit cells across these thin slabs prevents the direct application of continuous medium models for its characterization. The main aim of this contribution is to provide a rigorous model for these structures, also clarifying the usefulness of continuous medium approach for their characterization. The proposed model is a generalization of the classical Lorentz procedure to two dimensions and is able to deal with electrically thin slabs made of small resonant closed current loops. The obtained results are validated by full-wave electromagnetic simulations and compared with the continuous model approximation of the slab. © *2009 American Institute of Physics*. [DOI: 10.1063/1.3067788]

I. INTRODUCTION

One of the most promising applications of left-handed metamaterials is the Veselago–Pendry lens[1,2] made of a single slab of thickness d showing relative electric permittivity and magnetic permeability both equal to minus unity. In principle, this device will be able to reproduce, with any desired resolution, including subdiffraction resolution, the electromagnetic field on a given plane (source plane) located in front of the lens onto another plane (image plane) located behind the lens at a distance $2d$ from the source plane.[2] However, this effect is strongly limited by losses, which in practice reduces it to a near field effect. In fact, it can be shown (see Ref. 3 and references therein) that the minimum resolution attainable from a lossy slab, having the real parts of μ_r and ϵ_r both equal to minus unity, is given by

$$\Delta \geq \frac{2\pi d}{\ln(2/\delta)}, \tag{1}$$

where δ is the loss tangent of the slab. It is clear from Eq. (1) that $\Delta > d$ for any realistic metamaterial. This means that in order to obtain subdiffraction resolution ($\Delta < \lambda$) the slab thickness must be substantially smaller than the wavelength. In such case, electric and magnetic effects are decoupled and we are in the realm of the quasielectrostatics or the quasimagnetostatics. Therefore, only slabs with $\mu_r=-1$ or $\epsilon_r=-1$ are necessary in order to obtain subdiffraction resolution in the near field. The first possibility was actually analyzed in Ref. 2 and then experimentally demonstrated using a thin silver slab in Ref. 4. The second one was demonstrated in Ref. 5 using a ferrite slab.

Regarding imaging in the quasimagnetostatic limit, a promising application of metamaterial structures can be found in magnetic resonance imaging (MRI) for medical applications.[6–10] In Ref. 6 a hexagonal array of metallic Swiss rolls was used as a "magnetic flux guide" in order to translate MRI images from a source to a distant receiving coil. In Ref. 7 a Swiss roll $\mu_r=-1$ lens was proposed for MRI applications. In Refs. 8 and 9 the applications of split ring magnetoinductive lenses[8] for medical MRI were discussed. Later, a $\mu_r=-1$ lens made of split rings was proposed for the same application.[10] These applications include improvement of surface coil sensitivity and acceleration of measurement time in the frame of a parallel imaging process. Split ring lenses with $\mu_r=-1$ (Ref. 10) have the key advantages over Swiss-roll lenses[7] of three-dimensional (3D) isotropy and sensitivity to axial magnetic fields. With regard to magnetoinductive lenses,[8,9] split ring $\mu_r=-1$ lenses[10] have more complicated design, but this may be compensated by smaller losses and improved sensitivity coming from the fact that they do not operate at the split ring resonance, but well above it, in the negative permeability frequency range.

Since nuclear MRI takes place in the megahertz frequency range, a cubic array of capacitively loaded rings (CLRs) (Ref. 11) is a suitable design in order to approach ideal $\mu_r=-1$ lenses in practice (CLRs were already used for magnetoinductive lenses[8] operating in the same frequency range). Since losses in the metamaterial are essentially given by losses in its constitutive elements and vary inversely with the electrical size of these elements,[12] it is desirable from this point of view to use electrically big CLRs for the design. On the other hand, since according to Eq. (1) the minimum resolution cannot be made smaller than the slab thickness, there is no reason to use more than two or three periods along the slab width. From these considerations it comes out that the better design for the implementation of an artificial $\mu_r=-1$ lens for MRI applications contains only a few periods along the slab thickness. Such system, however, can hardly be considered as a continuous medium and a specific description must be developed in order to rigorously model its behavior.

According to the previous discussion, the main aim of this work will be to develop a specific model for the analysis of electrically thin periodic slabs of resonant split rings

[a]Electronic mail: l_jelinek@us.es.
[b]Electronic mail: marques@us.es.
[c]Electronic mail: freire@us.es.

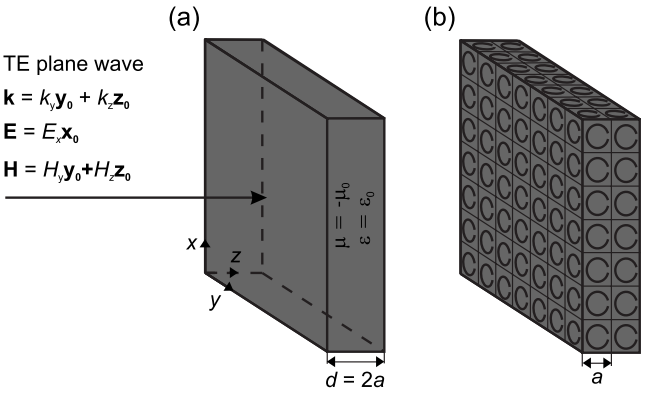

FIG. 1. (a) Ideal slab of an effective magnetic medium with $\mu=-\mu_0$. (b) A sketch of the proposed CLR implementation.

[which may include the aforementioned CLRs, as well as split ring resonators (SRRs) (Ref. 13) or other similar elements] with the sight on imaging applications. At the present state of the art it is possible to find, apart from the specific models developed for the analysis of magnetoinductive lenses,[8,9] some attempts of homogenization of thin metamaterial slabs or layers. One of the directions is the analytical calculation of the interaction constant inside double dipole arrays,[14,15] which finally leads to the definition of the effective material parameters for thin metamaterial slabs.[16] This method is not appropriate for the proposed application because it only takes into account normal incidence. Furthermore, it was developed for point dipole scatterers, which is not appropriate for the analysis of practical lenses with strongly coupled elements. Other possibility of homogenization of thin slabs was proposed in Ref. 17. This method derives the effective material parameters of a slab from the effective material parameters of a 3D infinite lattice. Also this method has two drawbacks for our purpose. First, the homogenization of a 3D lattice is in many cases of the same difficulty as the homogenization of a slab. Second, in order to calculate the transmission and reflection by a slab, spatial dispersion has to be taken into account.

To overcome the difficulties of the aforementioned approaches we will develop a model, which essentially is a kind of two-dimensional (2D) generalized Lorentz procedure including a detailed analysis of the magnetoinductive couplings between nearest neighbors. The results obtained from this model will be compared with those obtained from full-wave electromagnetic simulations in order to validate the analysis. They will also be compared with the results obtained from the continuous medium approach in order to find the limits of such approximation.

II. THE CONTINUOUS MEDIUM APPROACH

Figure 1(a) shows an ideal $\mu_r=-1$ lens for MRI applications. A practical implementation of this lens using CLRs, which, according to our previous discussion, has only two periods along the slab thickness, is sketched in Fig. 1(b). In order to find the effective parameters of the ideal lens in Fig. 1(a) we can follow the homogenization procedure developed in Ref. 18 [Eq. (13)], which takes into account magnetoinductive couplings between rings. Let us then suppose that this homogenization procedure applies and let us compute the transfer function of the lens, that is, the transmission coefficient between two planes at opposite sides of the lens, separated by a distance $2d$, where d is the lens width. Clearly, in the ideal case of $\mu_r=-1$, this transfer function must be equal to unity for any value of the transverse wave number k_y of the incident wave.

As mentioned above, the lens is supposed to operate in the quasimagnetostatic limit, where all fields are almost purely composed of evanescent TE modes. Let us then analyze the incidence of a TE plane wave, evanescent in the z-direction, on the slab in Fig. 1(a). Fields of such wave are

$$\mathbf{E}_0^{\text{inc}} = E_0^{\text{inc}} e^{j(k_y y + k_z z)} \mathbf{x}_0,$$

$$\mathbf{H}_0^{\text{inc}} = \frac{E_0^{\text{inc}}}{\omega\mu_0}(-k_z \mathbf{y}_0 + k_y \mathbf{z}_0) e^{j(k_y y + k_z z)}, \tag{2}$$

where $k_z=\sqrt{k_0^2-k_y^2}$, with $\text{Re}(k_z)<0$ and $\text{Im}(k_z)>0$. Taking the reference planes on the source and image planes (i.e., at two parallel planes located at both sides of the lens and separated by a distance $2d=4a$) the transmission coefficient of the lens can be written as

$$T = \frac{4\mu_r \frac{k_{zs}}{k_z} e^{jk_z d}}{\left(\frac{k_{zs}}{k_z}+\mu_r\right)^2 e^{-jk_{zs}d} - \left(\frac{k_{zs}}{k_z}-\mu_r\right)^2 e^{jk_{zs}d}}, \tag{3}$$

where $k_{zs}=\sqrt{\mu_r k_0^2 - k_y^2}$ is the longitudinal wave number inside the slab with $\text{Re}(k_{zs})<0$ and $\text{Im}(k_{zs})>0$. Making use of this approach, we have designed a $\mu_r=-1$ split ring lens for operation in a MRI 1.5 T machine ($f\approx 63.85$ MHz) according to the design sketched in Fig. 1(b) with the lattice constant $a=15$ mm. The CLRs were made of copper with metallic strips etched on a nonmagnetic dielectric board. The CLRs were loaded with lumped capacitors with normalized capacitance $C/(a\epsilon_0)=354$ (470 pF). The normalized mean radius of the CLRs was $r_0/a=0.329$ (4.935 mm) and the normalized width of the strips was $w/a=0.145$ (2.17 mm). The self-inductance of the CLRs was obtained from the measured value of the frequency of resonance in free space, whose normalized value was $k_0 a=0.0199$ (63.28 MHz). From this value, the CLR self-inductance $L=\omega_0^2/C$ was computed, having the normalized value $L/(a\mu_0)=0.714$ (13.5 nH). By measurement of the quality factor of the resonator, the normalized resistance $R/(\omega_0 L)=0.008\,69$ (0.0465 Ω), which includes the effects of the ring and the capacitor, was obtained. The permeability of a simple cubic lattice of such SRRs was then calculated using the homogenization procedure developed in Ref. 18 [Eq. (13)], and introduced in Eq. (3) in order to compute the transfer function of the lens. It is worth to note that strictly speaking, the analyzed CLR arrangement is not isotropic as it does not follow the necessary symmetries[19] due to the asymmetric location of the capacitors on the rings. However, the electrical size of the CLRs is so small (diameter/$\lambda=1/394$) that they can be practically seen as resonant closed current loops, supporting a uniform current distribution. Therefore, the analysis reported in Ref. 18 can be applied to the proposed structure.

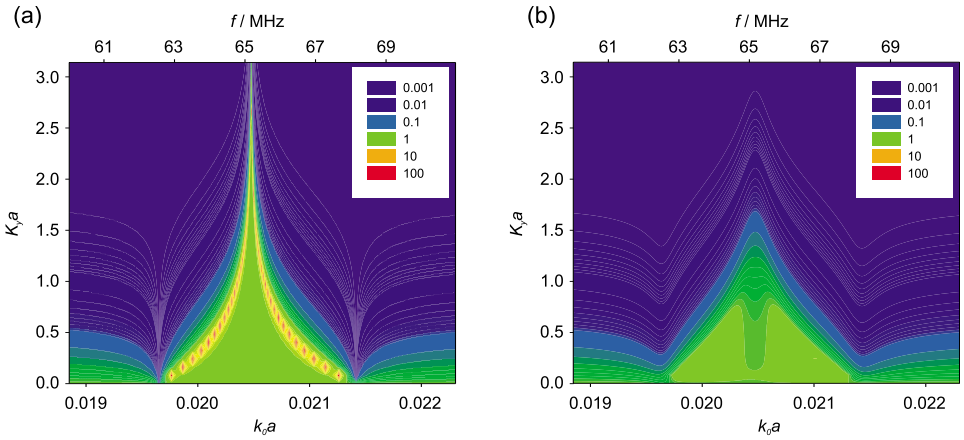

FIG. 2. (Color online) Transfer function through the $\mu_r=-1$ lens of Fig. 1 calculated using the continuous medium model in Ref. 18. (a) Losses are ignored ($R=0\ \Omega$). (b) Realistic losses ($R=0.0465\ \Omega$) are included in the model.

The computed amplitude of the transmission coefficient (3) is plotted in Fig. 2, as a function of the normalized frequency k_0a and the normalized transverse wave number k_ya. In the lossless case it can be seen that the transmission coefficient forms a flat valley between two steep cliffs, which corresponds to the surface waves that can be excited at both interfaces of the lens.[8] The frequency bandwidth of the valley increases from zero width at $k_ya=\pi$ to some finite width when the incident wave exhibits normal incidence. The transmission coefficient inside the entire valley has a value very close to unity, which reflects the imaging properties of the slab. The middle frequency of the valley corresponds to permeability $\mu_r=-1$. When realistic losses are included, the transfer function is strongly affected: both cliffs disappear (for smaller losses, for instance, $R=0.01\ \Omega$, we can still find some trace of them) and the spatial bandwidth (the allowed values of k_ya) becomes smaller. Since the resolution of the lens is limited by the minimum value of the allowed transverse wavelength $\lambda_y=2\pi/k_y$, the presence of losses reduces the resolution of the lens in agreement with our previous discussion. Nevertheless, the results shown in Fig. 2 are still very promising for MRI applications, as it will be shown in Sec. IV. However, as it was mentioned above, this conclusion is conditioned by the validity of the continuous medium model, which is not clear for the analyzed structure. In Sec. III we will develop a more accurate model and compare the results with those obtained in this section.

III. THE THIN SLAB MODEL

In this section a theoretical model of electrically thin slabs made of 2D periodic arrays of SRRs will be developed. The model will be particularized for the specific geometry discussed in Sec. II. However, it will become apparent that the analysis can be easily generalized to other similar configurations, including one or more layers of resonant current loops. The only limitations are a small electrical size of the loops and slab thickness. In our particular example, the slab is composed of a regular array of the unit cells shown in Fig. 3, which are periodically arranged in a square lattice of periodicity a over the x-y plane. It can be seen that each unit cell contains seven resonators (in our specific example they are CLRs, but other configurations, such as small SRRs, can also be considered). Figure 3(b) shows the current loop model of the real structure in Fig. 3(a), where it is assumed that each loop forms an *RLC* circuit[20] having self-impedance $Z_0=1/(j\omega C)+j\omega L+R$.

A. Circuit model of the slab

Let us assume now the incident wave (2) impinging on the slab. This polarization was selected due to the particular purpose of the example; however the analysis can be easily modified for incident plane waves of any polarization and phase shift in any direction. According to the model, each unit cell of the slab is described by a current vector $\mathbf{I}^{mn}$, where superindices m and n indicate the location of the unit cell in the x-y plane. Due to the assumed form of the incident field it is $\mathbf{I}^{mn}=\mathbf{I}^{00}e^{jk_yna}$. The currents in the unit cell at origin are driven by the magnetic flux across the different loops according to

$$Z_0 I_i^{00} = -j\omega\Phi_i^{00}, \quad i=1,\ldots,7, \tag{4}$$

where the magnetic flux Φ_i^{00} through the loops includes the flux of the external magnetic field as well as the magnetic flux created by all other loops in the lattice. Therefore, it can be then written that

$$\Phi_i^{00} = \Phi_i^{\text{ext}} + \sum_{j\neq i} M_{ij}^{00} I_j^{00} + \sum_{mn\neq 00}\sum_{j} M_{ij}^{mn} I_j^{mn}, \tag{5}$$

where M_{ij}^{mn} is the mutual inductance between ith loop in 00th cell and jth loop in mnth cell, and the summations extend over all the unit cells. Although Eq. (5) is formally correct, the last series are only conditionally convergent and cannot be used in practice. To overcome this difficulty, the well known Lorentz local field procedure[21] will be applied. This procedure, which for 3D structures leads to the well known

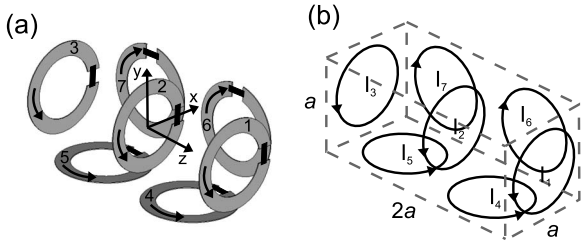

FIG. 3. (a) Considered unit cell made of CLRs. (b) Current loop model of the unit cell.

Clausius–Mossotti formula, has been successfully applied in the past to the analysis of 3D metamaterial structures (see, for instance, Ref. 3 and references therein) and, more recently, it has been applied to the analysis of 3D metamaterials made of resonant current loops.[18] In this paper, a straightforward generalization of this procedure to the analyzed 2D structure will be applied to compute the last summation in Eq. (5).

Following the aforementioned Lorentz approach, the whole metamaterial is divided in two regions: inside and outside a circle (actually a flat cylinder) of radius R around the 00th unit cell, i.e.,

$$\Phi_i^{00} = \Phi_i^{\text{ext}} + \sum_{j\neq i} M_{ij}^{00} I_j^{00} + \sum_j I_j^{00} \sum_{\substack{mn\neq 00 \\ m^2+n^2<R^2/a^2}} M_{ij}^{mn} e^{jk_y na} + \sum_j M_{ij}^{\infty} I_j^{00}, \tag{6}$$

where the term $\Sigma_j \sqrt{M_{ij}^{\infty} I_j^{00}}$ represents the magnetic flux coming from all the loops outside the circle.

Substitution of Eq. (6) into Eq. (4) then gives

$$(Z_0 \bar{\mathbf{1}} + j\omega \overline{\mathbf{M}} + j\omega \overline{\mathbf{M}}^{\infty}) \mathbf{I}^{00} = -j\omega \mathbf{\Phi}^{\text{ext}},$$

$$M_{ii} = \sum_{\substack{mn\neq 00 \\ m^2+n^2<R^2/a^2}} M_{ii}^{mn} e^{jk_y na},$$

$$M_{\substack{ij \\ i\neq j}} = M_{ij}^{00} + \sum_{\substack{mn\neq 00 \\ m^2+n^2<R^2/a^2}} M_{ij}^{mn} e^{jk_y na}. \tag{7}$$

This equation can be solved provided $\overline{\mathbf{M}}$, $\overline{\mathbf{M}}^{\infty}$, and the external magnetic flux $\mathbf{\Phi}^{\text{ext}}$ are known. Calculation of matrix $\overline{\mathbf{M}}$ is straightforward as its terms are given by summations of mutual inductances between two current loops, which are explicitly calculated in Appendix A. The expression for $\overline{\mathbf{M}}^{\infty}$ will be given in Sec. III C, assuming that the radius R is big enough so that the contribution coming from all the unit cells outside the circle can be seen as a continuous distribution of magnetization. The details of these computations are left to Sec. III C and to Appendix B; however, it is worth to mention that the proposed procedure avoids all the problems related to the slow convergence of the last summation in Eq. (5) because all series and integrals involved in the final expressions will be finite.

B. Transmission and reflection coefficient of the slab

The scattering of a plane wave by the considered slab is characterized by the transmission T and reflection R coefficients. At the present stage of the analysis, Eq. (7) only gives the currents on the loops along the periodic array. In order to calculate T and R, the far field radiated by the loops has to be calculated. In the far field region, the lens can be seen as seven parallel magnetized surfaces, each of them carrying the magnetization connected to each one of the seven loops in the unit cell, altogether with its periodic repetitions along the slab. Magnetization of each surface has the form

$$\mathbf{M} = \mathbf{M}_0 e^{jk_y y} \delta(z - z_i), \tag{8}$$

where z_i stands for the location of the layer along the z axis, that is, $z_1=a$, $z_2=0$, $z_3=-a$, $z_4=z_6=a/2$, and $z_5=z_7=-a/2$.

Radiation of these sources can be easily obtained by direct inversion of Maxwell equations. Assuming a magnetization layer at $z=z_i$ and $\mathbf{B}=\mu_0(\mathbf{H}+\mathbf{M})$, this results in

$$E_x = \frac{j\omega\mu_0}{2}\left(\frac{k_y M_{0z}}{k_z} - M_{0y}\,\text{sgn}(z-z_i)\right) e^{jk_y y} e^{jk_z|z-z_i|},$$

$$E_y = \frac{jk_0^2 M_{0x}}{2\omega\varepsilon_0}\text{sgn}(z-z_i) e^{jk_y y} e^{jk_z|z-z_i|},$$

$$E_z = -\frac{jk_y k_0^2 M_{0x}}{2\omega\varepsilon_0 k_z} e^{jk_y y} e^{jk_z|z-z_i|},$$

$$H_x = \frac{-k_0^2 M_{0x}}{2jk_z} e^{jk_y y} e^{jk_z|z-z_i|},$$

$$H_y = \frac{j}{2}[-k_y M_{0z}\,\text{sgn}(z-z_i) + k_z M_{0y}] e^{jk_y y} e^{jk_z|z-z_i|},$$

$$H_z = \frac{jk_y}{2}\left(\frac{k_y M_{0z}}{k_z} - M_{0y}\,\text{sgn}(z-z_i)\right) e^{jk_y y} e^{jk_z|z-z_i|} - M_{0z} e^{jk_y y}\delta(z-z_i). \tag{9}$$

Now, according to the indices in Fig. 3(b), it can be easily realized that only surfaces corresponding to loops 1, 2, 3, 4, and 5 contribute to the radiated E_x field component through

$$E_x^{1,2,3,4,5} = \frac{j\omega\mu_0 A}{2a^2}\left[\frac{k_y}{k_z} I_1 e^{jk_z|z-a|} + \frac{k_y}{k_z} I_2 e^{jk_z|z|} + \frac{k_y}{k_z} I_3 e^{jk_z|z+a|} - \text{sgn}\left(z-\frac{a}{2}\right) I_4 e^{jk_z|z-a/2|} - \text{sgn}\left(z+\frac{a}{2}\right) I_5 e^{jk_z|z+a/2|}\right] e^{jk_y y}, \tag{10}$$

and only surfaces corresponding to loops 6 and 7 contribute to the radiated E_y and E_z field components through

$$E_y^{6,7} = \frac{jk_0^2 A}{2\omega\varepsilon_0 a^2} e^{jk_y y}\left[\text{sgn}\left(z-\frac{a}{2}\right) I_6 e^{jk_z|z-a/2|} + \text{sgn}\left(z+\frac{a}{2}\right) I_7 e^{jk_z|z+a/2|}\right],$$

$$E_z^{6,7} = -\frac{jk_y k_0^2 A}{2\omega\varepsilon_0 k_z a^2} e^{jk_y y}(I_6 e^{jk_z|z-a/2|} + I_7 e^{jk_z|z+a/2|}), \tag{11}$$

where A states for the surface of the current loop.

Now, taking into account the presence of the incident wave, the reflection and transmission coefficients for the reference planes $z=-2a$ and $z=2a$ are given by

$$R^{xx} = \frac{E_x^{1,2,3,4,5}(z=-2a)}{E_0^{\text{inc}} e^{j(k_y y - 2k_z a)}} = \frac{j\omega\mu_0 A}{2a^2 E_0^{\text{inc}}}\left(\frac{k_y}{k_z} I_1 e^{2jk_z a} + \frac{k_y}{k_z} I_2 e^{jk_z a} + \frac{k_y}{k_z} I_3 + I_4 e^{3jk_z a/2} + I_5 e^{jk_z a/2}\right) e^{3jk_z a},$$

$$R^{yx} = \frac{E_y^{6,7}(z=-2a)}{E_0^{\text{inc}} e^{j(k_y y - 2k_z a)}} = \frac{-jk_0^2 A}{2\omega\varepsilon_0 a^2 E_0^{\text{inc}}}(I_6 e^{-jk_z a/2} + I_7 e^{jk_z a/2}),$$

$$R^{zx} = \frac{E_z^{6,7}(z=-2a)}{E_0^{\text{inc}} e^{j(k_y y - 2k_z a)}} = \frac{jk_y k_0^2 A}{2\omega\varepsilon_0 k_z a^2 E_0^{\text{inc}}}(I_6 e^{-jk_z a/2} + I_7 e^{jk_z a/2}),$$

$$T^{xx} = \frac{E_x^{1,2,3,4,5}(z=2a) + E_0^{\text{inc}} e^{j(k_y y + 2k_z a)}}{E_0^{\text{inc}} e^{j(k_y y - 2k_z a)}}$$

$$= \frac{j\omega\mu_0 A}{2a^2 E_0^{\text{inc}}}\left(\frac{k_y}{k_z} I_1 + \frac{k_y}{k_z} I_2 e^{jk_z a} + \frac{k_y}{k_z} I_3 e^{2jk_z a} - I_4 e^{jk_z a/2} - I_5 e^{3jk_z a/2}\right) e^{3jk_z a} + e^{4jk_z a},$$

$$T^{yx} = \frac{E_y^{6,7}(z=2a)}{E_0^{\text{inc}} e^{j(k_y y - 2k_z a)}} = -R^{yx} e^{4jk_z a},$$

$$T^{zx} = \frac{E_z^{6,7}(z=2a)}{E_0^{\text{inc}} e^{j(k_y y - 2k_z a)}} = R^{zx} e^{4jk_z a}. \tag{12}$$

In Eq. (12) superindices sign the co- and cross-polar components. The presence of cross-polar components, not found in homogeneous material slabs, is a consequence of the lack of periodicity in the z-direction. The transmission and reflection coefficients for the cross-polarized wave are, however, very small in the analyzed structure, as it will be shown in Sec. IV.

C. Calculation of the magnetic flux created by far neighbors

The last step before using Eq. (7) to calculate the induced currents and, subsequently, T^{ij} and R^{ij} coefficients, is the calculation of matrix $\overline{\mathbf{M}}^{\infty}$, which represents the coupling of each unit cell with its far neighbors. For this purpose we must evaluate the magnetic field over the unit cell at origin created by unit cells outside a circular hole of radius R. This situation is illustrated in Fig. 4.

Let us assume, following the procedure outlined in Sec. III A, that the hole is big in comparison to unit cell ($R \gg a$), that the unit cell is electrically small ($k_0 a \ll 1$, $k_y a \ll 1$), and that the slab is electrically thin ($k_0 d \ll 1$). In such case it is possible to say that the field over the unit cell at origin, created by neighbors outside of the hole, is almost uniform. Therefore, the magnetic flux through the loops of the unit cell will be $\Phi_i \approx A\mu_0 \mathbf{n}_i \cdot \mathbf{H}^M(0,0,0)$, where $\mathbf{n}_i$ is the normal to the ith loop and $\mathbf{H}^M(0,0,0)$ is the magnetic intensity at origin. Furthermore, since the slab is electrically thin, it can be said that the field $\mathbf{H}^M(0,0,0)$ is radiated by a surface with magnetization

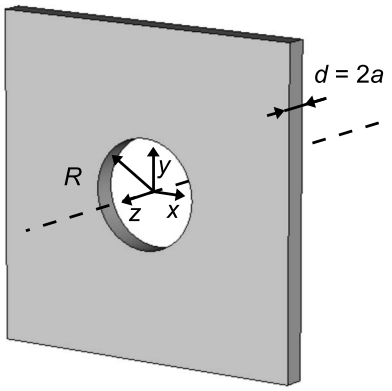

FIG. 4. Illustration of the slab with a hole of radius R.

$$\mathbf{M} = A\frac{(I_6 + I_7)\mathbf{x}_0 + (I_4 + I_5)\mathbf{y}_0 + (I_1 + I_2 + I_3)\mathbf{z}_0}{a^2} e^{jk_y y}\delta(z)$$

$$= \mathbf{M}_0 e^{jk_y y}\delta(z), \tag{13}$$

having a circular hole of radius R at the center. It may seem that the field $\mathbf{H}^M$ can be calculated by using free space Green's function for magnetic currents[22] and integrating over the surface with the hole. Although this is possible, it has to be taken into account that such approach leads to very poorly convergent integrals that prevent any numerical solution. This approach was used, for example, in Ref. 23 in case of $k_y = 0$, where the poor convergence was overcome by finding an analytical solution. Unfortunately, in the general case of $k_y \neq 0$ there is no closed form solution of such integrals, which prevents the generalization of such procedure. There is, however, another possible approach that can be described as follows: calculate the field created by a magnetized annulus of outer radius R and inner radius ϵ and subtract it from the field created by a magnetized surface with a hole of radius ϵ, assuming that ϵ is negligibly small. Making then the limit $\epsilon \to 0$ leads to the desired field $\mathbf{H}^M$. This procedure slightly differs from the standard Lorentz procedure since the field created by a surface of uniform magnetization has a singularity on the surface. This singularity is avoided by the subtraction of the fields created by a small circle of radius $\epsilon \to 0$. The advantage of this procedure is that since $\epsilon \to 0$, the magnetization of this last disk can be considered uniform, and therefore the fields can be easily computed. The mathematical details of outlined procedure can be found in Appendix B, where it is shown that

$$\overline{\mathbf{M}}^{\infty} = \frac{\mu_0 A^2}{a^2}\begin{bmatrix} F_z^{\infty} & F_z^{\infty} & F_z^{\infty} & 0 & 0 & 0 & 0 \\ F_z^{\infty} & F_z^{\infty} & F_z^{\infty} & 0 & 0 & 0 & 0 \\ F_z^{\infty} & F_z^{\infty} & F_z^{\infty} & 0 & 0 & 0 & 0 \\ 0 & 0 & 0 & F_y^{\infty} & F_y^{\infty} & 0 & 0 \\ 0 & 0 & 0 & F_y^{\infty} & F_y^{\infty} & 0 & 0 \\ 0 & 0 & 0 & 0 & 0 & F_x^{\infty} & F_x^{\infty} \\ 0 & 0 & 0 & 0 & 0 & F_x^{\infty} & F_x^{\infty} \end{bmatrix}, \tag{14}$$

where F_x^{∞}, F_y^{∞}, and F_z^{∞} are given by integrals (B8), which can be easily evaluated.

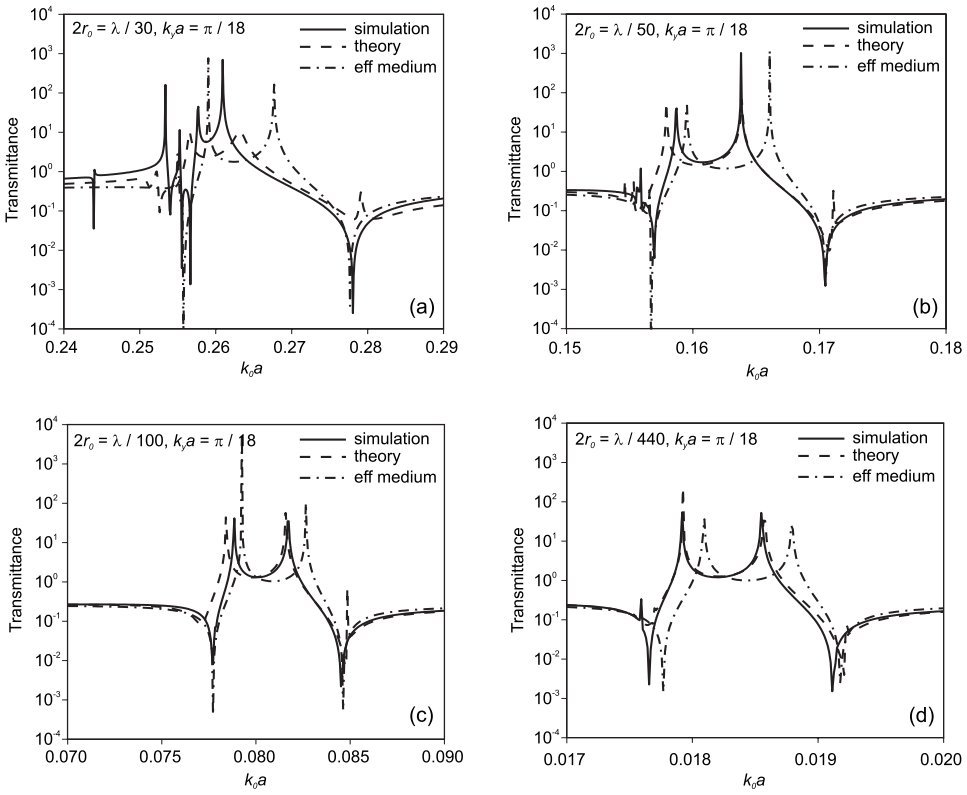

FIG. 5. Amplitude of the transmission coefficient for several electrical sizes of the CLRs in the lens of Fig. 1(b). The transmission coefficient was obtained by simulation (solid lines), theoretical model of Sec. III (dashed lines), and effective medium model (dashed-doted lines). The considered normalized transversal wave number is $k_y a = \pi/18$ in all figures.

IV. NUMERICAL VALIDATION AND COMPARISON WITH THE CONTINUOUS MEDIUM MODEL

In this section the results of the model developed through Sec. III will be compared to full-wave numerical simulations, carried out by the numerical *CST Microwave Studio* electromagnetic solver. The comparison will be provided via the calculated transmission coefficient between planes $z=-2a$ and $z=2a$ and the reflection coefficient at plane $z=-2a$. For all the following calculations of the coupling matrices $\overline{\mathbf{M}}^{\infty}$ and $\overline{\mathbf{M}}$ a radius $R=10a$ will be used. The simulated slab is made of CLRs with normalized mean radius $r_0/a=0.34$ and normalized width $w/a=0.13$. The normalized self-inductance $L=\omega^2/C$ was computed from the simulated frequency of resonance for several values of the capacitance C, and the value $L/(a\mu_0)=0.79$ was obtained. The losses in CLRs will be neglected at this moment so that all the resonance peaks are well visible.

First of all, the limits of the proposed model will be studied. For this purpose the capacitance of the CLRs is varied so that the mean diameter of the CLRs at resonance is $d/\lambda = 1/30$, 1/50, 1/100, and 1/440. The transmission coefficients for all the above situations obtained from the theoretical model, full-wave simulations, and effective medium model (see Sec. II) are depicted in Fig. 5. In all plots of Fig. 5 a normalized transversal wave number $k_y a=\pi/18$ was imposed. The plots for CLRs with $d/\lambda=1/30$ are depicted in Fig. 5(a). It can be seen that although the theoretical model reproduces the simulation better than the effective medium model, the quantitative agreement is very poor. This is expected since it is known[24] that the current induced on a conducting loop can be considered approximately uniform only if the circumference of the loop is smaller than $\lambda/10$. Therefore, the quantitative disagreements can be attributed to the imprecise assumption of a uniform current over the CLRs. This hypothesis is confirmed by the remaining panels of Fig. 5, where it can be clearly observed that as the CLRs become electrically smaller, the quantitative agreement between theory and simulation improves, reaching a practically perfect matching in Fig. 5(d). Noticeably, Fig. 5 also shows that the effective medium model provides a reasonable first order approximation for small CLRs, even though it shows a systematic frequency shift with regard to simulations. This frequency shift is present for any electrical size of the CLRs. Therefore it seems to be a consequence of the small number of unit cells through the slab, regardless of the size of the CRLs.

After the validation of the proposed model, the analysis will be focused on the slab made of CLRs with $d/\lambda = 1/440$, which is close to the slab proposed in Sec. II for MRI applications. To study the imaging properties of this slab, the transmission coefficient will be plotted for several values of the transversal phase shift. Figure 6(a) shows the result of the effective medium model and Fig. 6(b) shows the results of the model of Sec. III. As it was already mentioned in Sec. II, a $T\approx 1$ valley appears between two peaks in both cases. These peaks are approaching each other when the transverse phase shift increases; however it can be seen that there is always a region common to all curves. When dealing with effective medium model, this common region precisely corresponds with permeability around $\mu_r=-1$ and lies just in the middle between both peaks. The model in Sec. III corrects this scenario, showing that this common region is shifted to lower frequencies when the transverse phase shift increases and it is no more centered. However, in both cases,

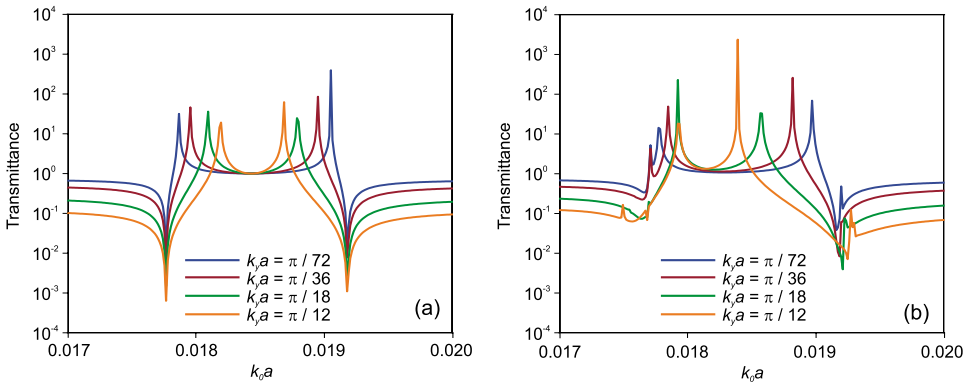

FIG. 6. (Color online) Amplitude of transmission coefficient for various transversal wave numbers obtained from the effective (a) medium model and the (b) model of Sec. III.

a frequency band of $T=1$ is present for moderate values of the transverse phase shift, which confirms the usefulness of the proposed design for MRI applications. Figure 7 shows the transmission and reflection coefficient of the lens. It reveals that an optimal point of minimum reflection appears just at the expected frequency of operation of the lens.

Finally, cross-polarization effects will be investigated. As it was already mentioned in Sec. III B, the analyzed slab produces not only copolar but also cross-polar components of the transmitted and reflected waves, as it can be seen from Eq. (12). In order to illustrate this effect, the transmission coefficients T^{xx} and T^{yx} are plotted in Fig. 8 for a normalized transversal wave number $k_y a = \pi/18$. It can be observed that especially in the region of interest, the cross-polar component is approximately two orders of magnitude smaller that the copolar one, having thus a negligible influence. Similar conclusions are reached for other transversal wave numbers.

V. CONCLUSION

A rigorous model has been proposed for the description of electrically thin metamaterial slabs made of resonant current loops. This includes electrically small capacitively loaded loops, SRRs, and other related configurations. This model allows for the computation of the transmission and reflection coefficients of any kind of propagative and/or evanescent incident plane wave, and is specifically well suited for the analysis of imaging applications of such slabs.

The reported model has been compared with numerical full-wave electromagnetic computations, and a good agreement has been found provided the hypothesis underlying the approximation is fulfilled. Specifically, it has been found that the proposed model remains valid, provided the size of the current loops is small enough to guarantee an approximately uniform current distribution along the loop. It has been also compared with the continuous medium model of the slab. The main conclusion of this comparison is that this last model provides a qualitative description of the electromagnetic behavior of the slab, even for thicknesses including a number of unit cells so small as two. Quantitatively, the continuous medium model fails by a small amount even for very small current loops, as a consequence of the small number of unit cells across the slab. In such situations, the main brawback of the continuous medium model is a non-negligible frequency shift in the transmission and reflection coefficients through the slab.

Applications of the above concepts in the design of metamaterial magnetic superlenses are envisaged. Specifically, medical applications in MRI can be foreseen. These applications could result in a meaningful increasing of the sensitivity of surface coils, reduction in image acquisition times, and improvement of parallel imaging techniques.

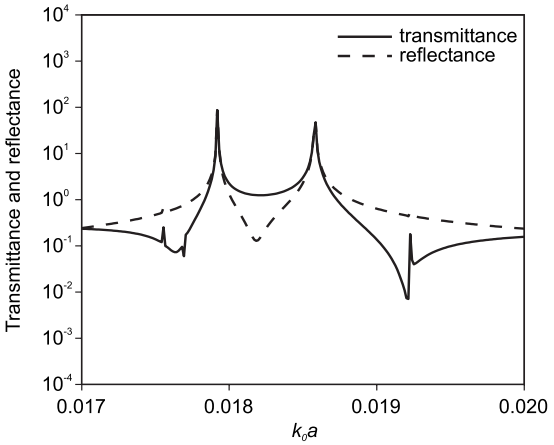

FIG. 7. Amplitude of transmission and reflection coefficient obtained from the model of Sec. III. The normalized transversal wave number is $k_y a = \pi/18$.

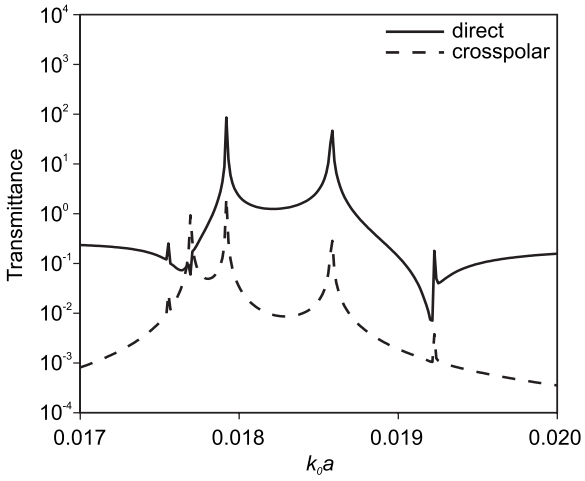

FIG. 8. Amplitude of transmission coefficient obtained from the model of Sec. III. The solid line represents direct copolar transmission, while dashed line represents transmission through cross-polar component. The normalized transversal wave number is $k_y a = \pi/18$.

ACKNOWLEDGMENTS

This work has been supported by the Spanish Ministerio de Educación y Ciencia under Project Nos. TEC2007-68013-C02-01/TCM and CSD2008-00066 as well as by the Spanish Junta de Andalucía under Project No. P06-TIC-01368.

APPENDIX A: MUTUAL INDUCTANCE OF TWO CURRENT LOOPS

For orthogonally oriented loops the parametrization of each current loop can be written as

$$x = r_0(n_z \cos\alpha + n_y \sin\alpha) + x_s,$$

$$y = r_0(n_z \sin\alpha - n_x \sin\alpha) + y_s,$$

$$z = r_0(n_y \cos\alpha + n_x \cos\alpha) + z_s,$$

$$\alpha \in (0, 2\pi), \tag{A1}$$

where n_x, n_y, and n_z are the components of the unit vector normal to the loop; x_s, y_s, and z_s are the coordinates of its center; and r_0 is the radius of the loop. The element of length in parametrization (A1) is given by

$$\mathbf{dl} = r_0[\mathbf{x}_0(-n_z \sin\alpha + n_y \cos\alpha) + \mathbf{y}_0(n_z \cos\alpha - n_x \cos\alpha) - \mathbf{z}_0(n_y \sin\alpha + n_x \sin\alpha)]d\alpha. \tag{A2}$$

The mutual inductance between two loops can now be calculated using the Neumann formula[22] as

$$M = \frac{\mu_0}{4\pi}\int_{l_2}\int_{l_1}\frac{e^{-jk_0\rho}}{\rho}\mathbf{dl}_1 \cdot \mathbf{dl}_2,$$

$$\rho = \sqrt{[x_1(\alpha_1) - x_2(\alpha_2)]^2 + [y_1(\alpha_1) - y_2(\alpha_2)]^2 + [z_1(\alpha_1) - z_2(\alpha_2)]^2}. \tag{A3}$$

For numerical calculations it is very convenient to rewrite Eq. (A3) as

$$M = \frac{\mu_0}{4\pi}\int_{l_2}\int_{l_1}\frac{e^{-jk_0\rho} - 1}{\rho}\mathbf{dl}_1 \cdot \mathbf{dl}_2 + \frac{\mu_0}{4\pi}\int_{l_2}\int_{l_1}\frac{1}{\rho}\mathbf{dl}_1 \cdot \mathbf{dl}_2. \tag{A4}$$

In Eq. (A4) the second integral (static part) does not depend on frequency and can be evaluated only once in whole frequency sweep. The first integral (dynamic part) has to be evaluated for each frequency. However the integrand is a very slow varying function (especially when $k_0\rho < \pi/2$, the integrand is practically a linear function), so only a few integration points are needed, which drastically fasten the calculation.

APPENDIX B: CALCULATION OF THE FIELD $\mathbf{H}^{M}(0,0,0)$

Let us assume a problem of negligibly small hole of radius ϵ cut in the magnetized surface. Such problem can be solved by subtracting the field of a disk of radius ϵ from the field of a full magnetization surface given by Eq. (9). Since the disk is negligibly small it is $k_y\epsilon \ll 1$, and the field in its center can be approximated by the field of a uniformly magnetized disk, a problem that is solved in Appendix C. It can be found that the field at the center of such disk is

$$H_x^{\text{disk }\epsilon} = \frac{-jk_0M_{0x}}{2} + \frac{1}{4}\left(jk_0 - \frac{1}{\epsilon}\right)M_{0x}e^{-jk_0\epsilon},$$

$$H_y^{\text{disk }\epsilon} = \frac{-jk_0M_{0y}}{2} + \frac{1}{4}\left(jk_0 - \frac{1}{\epsilon}\right)M_{0y}e^{-jk_0\epsilon},$$

$$H_z^{\text{disk }\epsilon} = -M_{0z}\delta(z=0) + \frac{1}{2}\left(jk_0 + \frac{1}{\epsilon}\right)M_{0z}e^{-jk_0\epsilon}. \tag{B1}$$

In Eq. (B1) it can be seen that the z-component of the field is divergent. However, it will be shown that this fact does not introduce any difficulty if the term $\delta(z=0)$ is treaded in symbolic way. Subtracting Eq. (B1) from Eq. (9) we can write the field in the center of hole of radius ϵ as

$$H_x^{\text{hole }\varepsilon} = \frac{-k_0^2M_{0x}}{2jk_z} + \frac{jk_0M_{0x}}{2} - \frac{1}{4}\left(jk_0 - \frac{1}{\varepsilon}\right)M_{0x}e^{-jk_0\varepsilon},$$

$$H_y^{\text{hole }\varepsilon} = \frac{j}{2}[-k_yM_{0z}\,\text{sgn}(z=0) + k_zM_{0y}] + \frac{jk_0M_{0y}}{2} - \frac{1}{4}\left(jk_0 - \frac{1}{\varepsilon}\right)M_{0y}e^{-jk_0\varepsilon},$$

$$H_z^{\text{hole }\varepsilon} = \frac{jk_y}{2}\left(\frac{k_yM_{0z}}{k_z} - M_{0y}\,\text{sgn}(z=0)\right) - \frac{1}{2}\left(jk_0 + \frac{1}{\varepsilon}\right)M_{0z}e^{-jk_0\varepsilon}. \tag{B2}$$

The problem of the terms $\text{sgn}(z=0)$ in Eq. (B2) can be solved as follows: assume that there is only magnetization M_{0z}. In such case there is an x-y magnetic wall at $z=0$ and H_y must vanish on it. This means that we can take $\text{sgn}(z=0)=0$ for H_y components. In a similar way, when there is only magnetization M_{0y}, there must be an x-y electric wall at $z=0$ and H_z must vanish on it. This means that we can take $\text{sgn}(z=0)=0$ for H_z component. Finally we obtain

$$H_x^{\text{hole }\varepsilon} = \left[\frac{jk_0^2}{2k_z} + \frac{jk_0}{2} - \frac{1}{4}\left(jk_0 - \frac{1}{\varepsilon}\right)e^{-jk_0\varepsilon}\right]M_{0x},$$

$$H_y^{\text{hole }\varepsilon} = \left[\frac{jk_z}{2} + \frac{jk_0}{2} - \frac{1}{4}\left(jk_0 - \frac{1}{\varepsilon}\right)e^{-jk_0\varepsilon}\right]M_{0y},$$

$$H_z^{\text{hole }\varepsilon} = \left[\frac{jk_y^2}{2k_z} - \frac{1}{2}\left(jk_0 + \frac{1}{\varepsilon}\right)e^{-jk_0\varepsilon}\right]M_{0z}. \tag{B3}$$

The final step is now to subtract from Eq. (B3) the field in the center of an annulus with outer radius R and inner radius ϵ. The field of such annulus can be solved by direct integration of the magnetic current Green's function, which leads to

$$H_x^{\text{annulus}} = \frac{M_{0x}}{2}\int_\varepsilon^R \left\{k_0^2\left(J_0(k_y\rho) - \frac{J_1(k_y\rho)}{k_y\rho}\right) + \frac{(1+jk_0\rho)}{\rho^2}\left(3\frac{J_1(k_y\rho)}{k_y\rho} - J_0(k_y\rho)\right)\right\}e^{-jk_0\rho}d\rho,$$

$$H_y^{\text{annulus}} = \frac{M_{0y}}{2}\int_\varepsilon^R \left\{k_0^2\frac{J_1(k_y\rho)}{k_y\rho} + \frac{(1+jk_0\rho)}{\rho^2}\left(2J_0(k_y\rho) - \frac{3J_1(k_y\rho)}{k_y\rho}\right)\right\}e^{-jk_0\rho}d\rho,$$

$$H_z^{\text{annulus}} = \frac{M_{0z}}{2}\int_\varepsilon^R \left\{k_0^2 - \frac{(1+jk_0\rho)}{\rho^2}\right\}J_0(k_y\rho)e^{-jk_0\rho}d\rho. \tag{B4}$$

Subtraction of Eq. (B4) from Eq. (B3) gives the field $H^M(0,0,0)$ at the center of the circular hole of radius R. The integrals in Eq. (B4) can be solved numerically; however the numerical solution is difficult due to the divergent behavior of the integrands for $\rho=0$ (note that it is assumed that $k_y\epsilon \ll 1$). However, this problem can be easily solved. The integrals in Eq. (B4) have a closed form solution in the case of $k_y=0$, which reads

$$G_x = \frac{M_{0x}}{4}\int_\varepsilon^R \left\{k_0^2 + \frac{(1+jk_0\rho)}{\rho^2}\right\}e^{-jk_0\rho}d\rho = \frac{M_{0x}}{4}\left\{\left(jk_0 - \frac{1}{R}\right)e^{-jk_0R} + \left(-jk_0 + \frac{1}{\varepsilon}\right)e^{-jk_0\varepsilon}\right\},$$

$$G_y = \frac{M_{0y}}{4}\int_\varepsilon^R \left\{k_0^2 + \frac{(1+jk_0\rho)}{\rho^2}\right\}e^{-jk_0\rho}d\rho = \frac{M_{0y}}{4}\left\{\left(jk_0 - \frac{1}{R}\right)e^{-jk_0R} + \left(-jk_0 + \frac{1}{\varepsilon}\right)e^{-jk_0\varepsilon}\right\},$$

$$G_z = \frac{M_{0z}}{2}\int_\varepsilon^R \left\{k_0^2 - \frac{(1+jk_0\rho)}{\rho^2}\right\}e^{-jk_0\rho}d\rho = \frac{M_{0z}}{2}\left\{\left(jk_0 + \frac{1}{R}\right)e^{-jk_0R} + \left(-jk_0 - \frac{1}{\varepsilon}\right)e^{-jk_0\varepsilon}\right\}. \tag{B5}$$

Now, we can add the right-hand part and subtract the left-hand part of Eq. (B5) from Eq. (B4), which leads to

$$H_x^{\text{annulus}} = \frac{M_{0x}}{2}\int_\varepsilon^R \left\{k_0^2\left(J_0(k_y\rho) - \frac{J_1(k_y\rho)}{k_y\rho} - \frac{1}{2}\right) + \frac{(1+jk_0\rho)}{\rho^2}\left(3\frac{J_1(k_y\rho)}{k_y\rho} - J_0(k_y\rho) - \frac{1}{2}\right)\right\}e^{-jk_0\rho}d\rho + \frac{M_{0x}}{4}\left\{\left(jk_0 - \frac{1}{R}\right)e^{-jk_0R} + \left(-jk_0 + \frac{1}{\varepsilon}\right)e^{-jk_0\varepsilon}\right\},$$

$$H_y^{\text{annulus}} = \frac{M_{0y}}{2}\int_\varepsilon^R \left\{k_0^2\left(\frac{J_1(k_y\rho)}{k_y\rho} - \frac{1}{2}\right) + \frac{(1+jk_0\rho)}{\rho^2}\left(2J_0(k_y\rho) - \frac{3J_1(k_y\rho)}{k_y\rho} - \frac{1}{2}\right)\right\}e^{-jk_0\rho}d\rho + \frac{M_{0y}}{4}\left\{\left(jk_0 - \frac{1}{R}\right)e^{-jk_0R} + \left(-jk_0 + \frac{1}{\varepsilon}\right)e^{-jk_0\varepsilon}\right\},$$

$$H_z^{\text{annulus}} = \frac{M_{0z}}{2}\int_\varepsilon^R \left\{k_0^2 - \frac{(1+jk_0\rho)}{\rho^2}\right\}\{J_0(k_y\rho) - 1\}e^{-jk_0\rho}d\rho + \frac{M_{0z}}{2}\left\{\left(jk_0 + \frac{1}{R}\right)e^{-jk_0R} + \left(-jk_0 - \frac{1}{\varepsilon}\right)e^{-jk_0\varepsilon}\right\}. \tag{B6}$$

Field (B6) is identical to Eq. (B4), but now all the integrands tend to zero for $\rho\to 0$ and all integrals in Eq. (B6) can be numerically evaluated without difficulty. Finally the subtraction of Eq. (B6) from Eq. (B3), taking into account Eq. (13), leads to

$$\overline{\mathbf{M}}^\infty = \frac{\mu_0 A^2}{a^2}\begin{bmatrix} F_z^\infty & F_z^\infty & F_z^\infty & 0 & 0 & 0 & 0 \\ F_z^\infty & F_z^\infty & F_z^\infty & 0 & 0 & 0 & 0 \\ F_z^\infty & F_z^\infty & F_z^\infty & 0 & 0 & 0 & 0 \\ 0 & 0 & 0 & F_y^\infty & F_y^\infty & 0 & 0 \\ 0 & 0 & 0 & F_y^\infty & F_y^\infty & 0 & 0 \\ 0 & 0 & 0 & 0 & 0 & F_x^\infty & F_x^\infty \\ 0 & 0 & 0 & 0 & 0 & F_x^\infty & F_x^\infty \end{bmatrix}, \tag{B7}$$

where

$$F_x^\infty = \left\{\left[\frac{jk_0^2}{2k_z} + \frac{jk_0}{2} - \frac{1}{4}\left(jk_0 - \frac{1}{R}\right)e^{-jk_0R}\right] - \frac{1}{2}\int_\varepsilon^R \left\{k_0^2\left[J_0(k_y\rho) - \frac{J_1(k_y\rho)}{k_y\rho} - \frac{1}{2}\right] + \frac{(1+jk_0\rho)}{\rho^2}\left[3\frac{J_1(k_y\rho)}{k_y\rho} - J_0(k_y\rho) - \frac{1}{2}\right]\right\}e^{-jk_0\rho}d\rho\right\},$$

$$F_y^{\infty} = \left\{ \left[\frac{jk_z}{2} + \frac{jk_0}{2} - \frac{1}{4}\left(jk_0 - \frac{1}{R} \right) e^{-jk_0 R} \right] - \frac{1}{2}\int_{\varepsilon}^{R} \left\{ k_0^2 \left[\frac{J_1(k_y\rho)}{k_y\rho} - \frac{1}{2} \right] + \frac{(1+jk_0\rho)}{\rho^2} \left[2J_0(k_y\rho) - \frac{3J_1(k_y\rho)}{k_y\rho} - \frac{1}{2} \right] \right\} e^{-jk_0\rho} d\rho \right\},$$

$$F_z^{\infty} = \left\{ \left[\frac{jk_y^2}{2k_z} - \frac{1}{2}\left(jk_0 + \frac{1}{R} \right) e^{-jk_0 R} \right] - \frac{1}{2}\int_{\varepsilon}^{R} \left[k_0^2 - \frac{(1+jk_0\rho)}{\rho^2} \right] [J_0(k_y\rho) - 1] e^{-jk_0\rho} d\rho \right\}. \quad \text{(B8)}$$

All integrals in Eq. (B8) converge even for $\epsilon=0$. Making $\epsilon \to 0$ leads to the exact solution.

APPENDIX C: MAGNETIC FIELD IN THE MIDDLE OF A UNIFORMLY MAGNETIZED DISK

Assume that the disk of radius ϵ carries a uniform magnetization

$$\mathbf{M} = \mathbf{M}_0 \delta(z). \quad \text{(C1)}$$

The magnetic intensity produced in the disk center will be obtained in two steps. First of all, setting $k_y=0$ in Eq. (9), we obtain the magnetic field intensity radiated by an infinite surface of magnetization $\mathbf{M}$,

$$H_x = \frac{-jk_0 M_{0x}}{2} e^{-jk_0|z|},$$

$$H_y = \frac{-jk_0 M_{0y}}{2} e^{-jk_0|z|},$$

$$H_z = -M_{0z}\delta(z). \quad \text{(C2)}$$

Then, it is assumed that there is a circular hole of radius ϵ on the surface of magnetization (C1). Since $k_y=0$, this problem can be solved directly by integration of the magnetic Green's function. Introducing polar coordinates and using the identity

$$\frac{\partial}{\partial\rho}\left(\frac{e^{-jk_0\rho}}{\rho} \right) = -\frac{1+jk_0\rho}{\rho^2} e^{-jk_0\rho},$$

it is found that the magnetic field intensity in the middle of the hole is

$$\mathbf{H} = \frac{1}{4}\left\{ -jk_0 \begin{bmatrix} 1 & 0 & 0 \\ 0 & 1 & 0 \\ 0 & 0 & 2 \end{bmatrix} + \frac{1}{\epsilon} \begin{bmatrix} 1 & 0 & 0 \\ 0 & 1 & 0 \\ 0 & 0 & -2 \end{bmatrix} \right\} \mathbf{M}_0 e^{-jk_0\epsilon}. \quad \text{(C3)}$$

Now, by subtracting Eq. (C3) from Eq. (C2) we can easily obtain the field in the middle of uniformly magnetized disk of radius ϵ.

[1] V. G. Veselago, Sov. Phys. Usp. **10**, 509 (1968).
[2] J. B. Pendry, Phys. Rev. Lett. **85**, 3966 (2000).
[3] R. Marqués, F. Martín, and M. Sorolla, *Metamaterials with Negative Parameters: Theory and Microwave Applications* (Wiley, New York, 2008).
[4] N. Fang, H. Lee, C. Sun, and X. Zhang, Science **308**, 534 (2005).
[5] R. Marqués, F. Mesa, and F. Medina, Appl. Phys. Lett. **86**, 023505 (2005).
[6] M. C. K. Wiltshire, J. B. Pendry, I. R. Young, D. J. Larkman, D. J. Gilderdale, and J. V. Hajnal, Science **291**, 849 (2001).
[7] M. C. K. Wiltshire, J. B. Pendry, and J. V. Hajnal, J. Phys.: Condens. Matter **18**, L315 (2006).
[8] M. J. Freire and R. Marqués, J. Appl. Phys. **100**, 063105 (2006).
[9] M. J. Freire and R. Marqués, J. Appl. Phys. **103**, 013115 (2008).
[10] M. Freire and R. Marqués, Proceedings of Metamaterials, Pamplona, Spain, 23–26 September 2008 (unpublished).
[11] S. A. Schelkunoff and H. T. Friis, *Antennas: Theory and Practice* (Wiley, New York, 1952).
[12] S. A. Cummer, B. I. Popa, and T. H. Hand, IEEE Trans. Antennas Propag. **56**, 127 (2008).
[13] J. B. Pendry, A. J. Holden, D. J. Robbins, and W. J. Stewart, IEEE Trans. Microwave Theory Tech. **47**, 2075 (1999).
[14] V. V. Yatsenko, S. I. Maslovski, S. A. Tretyakov, S. L. Prosvirnin, and S. Zouhdi, IEEE Trans. Antennas Propag. **51**, 2 (2003).
[15] S. Tretyakov, *Analytical Modeling in Applied Electromagnetics* (Artech House, Boston, MA, 2003).
[16] E. Saenz, P. Ikonen, R. Gonzalo, and S. Tretyakov, J. Appl. Phys. **101**, 114910 (2007).
[17] M. G. Silveirinha and C. A. Fernandes, Phys. Rev. E **75**, 036613 (2007).
[18] J. D. Baena, L. Jelinek, R. Marqués, and M. Silveirinha, Phys. Rev. A **78**, 013842 (2008).
[19] J. D. Baena, L. Jelinek, and R. Marqués, Phys. Rev. B **76**, 245115 (2007).
[20] R. Marqués, F. Medina, and R. Rafii-El-Idrissi, Phys. Rev. B **65**, 144440 (2002).
[21] H. S. Lorentz, Ann. Phys. **9**, 641 (1880).
[22] J. D. Jackson, *Classical Electrodynamics*, 3rd ed. (Wiley, New York, 1998).
[23] S. I. Maslovski and S. A. Tretyakov, AEU, Int. J. Electron. Commun. **53**, 135 (1999).
[24] C. A. Balanis, *Antenna Theory: Analysis and Design*, 2nd ed. (Wiley, New York, 1997), p. 950.